RSC Advances

PAPER

View Article Online
View Journal | View Issue

Cite this: *RSC Adv.*, 2025, **15**, 35109

Synthesis, crystal structure and properties of 3-picrylamino-1,2,4-triazole-nitric acid self-assembled energetic material

Xiaoyan Zhang,[a] Qisheng Zhang,[b] Yunshu Zhao,[a] Guiying Li,[a] Tiying Jiang,[a] Zhirong Suo,[a] Shanhu Sun *[a] and Li Su*[a]

The oxygen balance (OB) of energetic materials plays a critical role in determining the efficiency and effectiveness of energy release during combustion or detonation. To enhance the OB and comprehensive properties of 3-picrylamino-1,2,4-triazole (PATO), which is a high-energy and low-sensitivity explosive, this study employed a self-assembly strategy to combine nitric acid with PATO, resulting in a novel 3-picrylamino-1,2,4-triazole-nitric acid self-assembled energetic material (PATO-N). Its structure was characterized by single crystal X-ray diffraction, and the thermal decomposition properties and impact sensitivity were measured. The detonation performances were predicted by EXPLO5 and the OB was calculated based on its molecular formula. The results indicate that the self-assembly of PATO and HNO_3 effectively enhanced the explosive's OB (−67.7% to −44.6%)and promoted the completeness of the detonation reaction. PATO-N exhibits good thermal stability with an improved decomposition temperature of 315.9 °C. Its theoretical detonation velocity is 7.8 km s^{-1}, while the detonation pressure is 25.2 Gpa. PATO-N exhibited an impact sensitivity (H_{50}) exceeding 112.2 cm, classifying it as an insensitive energetic material.

Received 22nd July 2025
Accepted 17th September 2025

DOI: 10.1039/d5ra05291b

rsc.li/rsc-advances

1 Introduction

Energetic materials are a class of special substances that rapidly release energy and generate gas in a short time through their own redox reactions after being stimulated by a certain external environment, including explosives, pyrolite, propellants, *etc.*[1–3] Self-oxygenation is a basic characteristic of explosives. The oxygen balance (OB), defined as the oxygen surplus or deficit per unit mass of the explosive after complete oxidation of its combustible elements, is an important indicator for characterizing the explosive performance,[4] and is related to the detonation velocity, detonation pressure, detonation heat, and work capacity.[5] In the field of modern energetic materials, widely used elemental explosives generally exhibit negative OB. Such explosives include TNT (−74%),[6] RDX (−21.61%),[7] HMX (−22%),[8] and CL-20 (−10.95%).[9] A negative OB causes the explosive to produce incomplete oxide during the detonation process, reducing the energy release efficiency. Recently, in response to this important issue, studies have mainly conducted OB optimization research in three directions, with relevant findings reported in each. First, the introduction of oxygen-containing groups in the molecular skeleton of explosives regulates the molecular OB directly.[10–14] However, this method encounters challenges such as complex synthesis routes and long development cycles or it may affect the stability and safety of explosives. Second, the explosive and oxidant[15] are mechanically mixed in specific proportions to form composite explosives,[16–21] aiming to enhance energy release efficiency, such as thermobaric explosives.[22,23] However, mechanical mixing is challenging owing to the need for sophisticated technology and strict safety measures. Third, the supramolecular self-assembly of oxidizing molecules and explosives based on the self-assembly strategy is a promising modification method with simple operation and an environmentally benign process.

The self-assembly strategy refers to the spontaneous organization of different components through non-covalent interactions, such as hydrogen bonds, van der Waals forces, or π–π stacking, to form an ordered structure in the target material.[24,25] In early-stage research, hydrogen peroxide (H_2O_2), nitric acid (HNO_3), and perchloric acid ($HClO_4$) have been frequently employed in conjunction with explosives to improve the OB performance of explosives through self-assembly. For example, Song *et al.*[26] designed and prepared three self-assembled energetic materials by combining 2,4,6-tria-mino-1,3,5-triazine-1,3-dioxide (TTDO) and strong oxidizers (H_2O_2, HNO_3, $HClO_4$). The OB of the novel composite materials was noticeably improved, with 2,4,6-triamino-1,3,5-triazine-1,3-dioxide-HNO_3 self assembled energetic material (TTDON) exhibiting

[a]School of Materials and Chemistry, Southwest University of Science and Technology, Mianyang 621010, Sichuan, People's Republic of China. E-mail: shanhusun@126.com; suli@swust.edu.cn

[b]School of Environment and Resource, Southwest University of Science and Technology, Mianyang 621010, Sichuan, People's Republic of China

particularly outstanding performance, specifically achieving a high density of 2.047 g cm^{-3} and detonation performances (D_v = 9284 m s^{-1}, P = 41 GPa) comparable with those of HMX. Similarly, Jiang *et al.*[27] demonstrated that the self-assembly of triazene-bridged triazole with HNO_3 and $HClO_4$ produced energetic composites, among which the triazene-bridged triazole–$HClO_4$ (1 : 2) adduct exhibited optimal overall performance (OB = −10.5%, D = 8135 m s^{-1}, P = 29.3 GPa), surpassing TNT in terms of both detonation capability and safety. Furthermore, Liu *et al.*[28] reported that the supramolecular materials of 3-amino-4-(4,5-diamino-1,2,4-triazole-3-yl)-furazan (TATF) with strong acid (HNO_3, $HClO_4$) achieved detonation parameters approaching those of RDX while offering enhanced safety. In addition to the three oxidizing molecules of H_2O_2, HNO_3, and $HClO_4$, some studies have combined iodine-containing iodic acid (HIO_3) and periodic acid (H_5IO_6) with explosive molecules. Li *et al.*[29] prepared four iodine-rich self-assembled energetic materials. They found that these four materials exhibited better OB and detonation compared with TNT, suggesting their potential applicability as biocidal agents. Similarly, Yang *et al.*[30] synthesized 4,7-diaminotriazolo [4,5-*d*] pyridazine, and then prepared three self-assembled energetic materials with HNO_3, HIO_3, and $HClO_4$. They achieved excellent detonation performance, safety performance, and thermal stability. In summary, self-assembly is an effective and promising strategy for developing new energetic materials and improving the OB of explosives.

1,2,4-Triazole serves as a key structural component in high-performance energetic materials because of its high nitrogen content, significant enthalpy of formation, and optimal balance of energy and sensitivity.[31] It is extensively utilized in the design of heat-resistant, high-energy, and low-sensitivity compounds, for example, it serves as a key scaffold for constructing nitrogen-rich fused ring systems,[32–36] as an ideal precursor for energetic ionic salts,[37–39] and an excellent ligand for synthesizing high-energy metal complexes.[40] As a classical triazole-based energetic compound, 3-picrylamino-1,2,4-triazole (PATO) was first synthesized by Coburn in 1968.[41,42] It exhibits excellent thermal stability with a decomposition temperature exceeding 300 °C, low mechanical sensitivity (impact sensitivity H_{50} = 137 cm), and low production cost. These properties once made PATO a promising candidate as a substitute for the high-energy explosive TATB.[43–47] However, the negative OB (−67.7%) of PATO affects its energy output efficiency. In this study, PATO was combined with oxygen-rich oxidant HNO_3 to synthesize a new supramolecular energetic compound 3-picrylamino-1,2,4-triazole-nitric acid self-assembled energetic material (PATO-N) with the research background for the self-assembly of energetic materials and oxidants. The crystal structure of PATO-N was characterized by X-ray crystal diffraction (SXRD). Its thermal stability was investigated based on thermogravimetry-differential scanning calorimetry (TG-DSC) analysis, and its safety was evaluated through impact sensitivity (H_{50}). The detonation performances were computationally simulated using EXPLO5. Furthermore, the PATO-N stored at 50 relative humidity was characterized by powder X-ray diffraction. And the phase stability of PATO-N under specific storage conditions and its compatibility with the high-energy material CL-20 were also investigated (see supplementary information).

2 Experimental section

2.1 Materials

In this study, PATO was synthesized based on the study by Leonard[46] (Scheme S1). Phenol, nitric acid, sulfuric acid, and dimethylformamide were obtained from Chengdu Cologne Chemical Co., Ltd, while phosphorus oxychloride and 3-aminotriazole were obtained from Shanghai Aladdin Biochemical Technology Co., Ltd. CL-20 was self-synthesized in Southwest University of Science and Technology. All pharmaceutical reagents used in the experiment were of analytical grade and did not require further purification.

2.2 Preparation of PATO-N

The PATO (0.1 g, 0.338 mmol) was weighed and transferred into a 50 mL round-bottom flask. Distilled water (6 mL) was added, and the mixture was heated to 50% in an oil bath under stirring at 20 rpm. Subsequently, 6 mL of 68% (w/w) nitric acid was added dropwise to the PATO suspension using a rubber-tipped dropper. Upon complete addition, the PATO dissolved entirely, forming a yellow transparent solution, which was stirred continuously for 1 hour. Finally, the transparent solution was transferred to a 50 mL beaker, and yellow needle-like crystals were obtained after solvent evaporation at room temperature over one week. FTIR (KBr): 718, 1081, 1171, 1237, 1356, 1392, 1444, 1526, 1615, 3148, 3259; ^{1}H NMR (600 MHz, DMSO): δ 8.92 (s, 2H), 8.37 (s, 1H); HPLC-MS (ESI$^-$): m/z: 294.2 [M–H$^-$] (Fig. S4–6).

2.3 Characterization

The Fourier transform infrared spectra (FTIR) were recorded using a Nicolet-5700 spectrometer with KBr pellets in the range of 4000–400 cm^{-1}.

The nuclear magnetic resonance (NMR) spectra were obtained using the AVANCE 600 superconducting NMR spectrometer, with samples dissolved in DMSO-d6.

High-performance liquid chromatography-mass spectrometry (HPLC-MS) analyses were conducted using a Varian HPLC-MS 325 system.

The X-ray diffraction patterns (PXRD) of the samples were recorded using a PANalytical Empyrean X-ray diffractometer at 40 kV and 40 mA with Cu Kα radiation λ = 1.541874 Å.

Single-crystal X-ray diffraction (SC-XRD) was performed on a Bruker D8 Venture diffractometer using Mo Kα radiation (λ = 0.71073 nm) and ω–2θ scanning mode.

Thermogravimetry-differential scanning calorimetry (TG-DSC) measurements were carried out on a TA-SDT650 instrument over a temperature range from room temperature to 600 °C, at a heating rate of 10 °C min^{-1} under a nitrogen atmosphere.

The impact sensitivity was investigated on a WL-1 type impact sensitivity instrument according to the GJB772B standard method. About 30 mg of material for each sample was

placed in steel anvils and struck by a free falling 2.0 kg drop weight. Samples were tested for a 50% probability to detonate (H_{50}) when impacted from a specified height by using the up and down method.

3 Results and discussion

3.1 Crystal structure

The molecular surface electrostatic potential (ESP) of PATO was calculated using Gaussian 09, and the results are shown in Fig. 1(a). As can be seen, the lowest ESP value (−44 kcal mol^{-1}) was localized around the N–N bond of the azole ring in PATO suggesting significant electron density enrichment characteristics and strong nucleophilic ability in this region, which was the dominant hydrogen bond acceptor active site of the molecule. The highest positive ESP value (+56 kcal mol^{-1}) appeared near the N–H group of the azole ring, indicating pronounced electrophilicity at this site. This region serves as the key active site for the dominant hydrogen-bond donor in PATO. The crystal structure of PATO-N was characterized by SXRD, and the results are presented in Table 1. The supramolecular structure of PATO-N (1 : 1) belongs to the orthorhombic system, with space group $Pca2_1$ and density of 1.776 g cm^{-3}. When viewed along the *c*-axis, the PATO-N crystal exhibits a wavy lamellar stacking pattern (Fig. 1(b)). This structural feature arises from the non-coplanar arrangement of the benzene and azole rings in PATO, which creates interplanar voids accommodating the nitrate counterions. The unique wavy lamellar stacking helps to reduce external mechanical stimuli, while maintaining the crystalline stability caused by the hydrogen bonding networks, thereby ensuring the safety of the novel material. As shown in Fig. 1(c), the intermolecular hydrogen bonds in the PATO-N crystal mainly exist between two PATO molecules and between PATO and nitrate. Between two adjacent PATO molecules, the C–H on the azole ring acts as a hydrogen bond donor, and the oxygen atom in the –NO_2 group acts as a hydrogen bond acceptor to form a medium-strength hydrogen bond C_8–$H_8\cdots O_6$ (2.241 Å, 174.43°). Hydrogen bonding interactions between PATO and nitrate involve the N–H group on the PATO azole ring, which acts as a hydrogen bond donor, and the oxygen atom on the nitro group in the nitrate, which serves as a hydrogen bond acceptor, to form strong hydrogen bonds N_5–$H_5\cdots$O9 (1.840 Å, 167.95°) and N_6–$H_6\cdots O_8$ (1.829 Å, 172.74°). The N–H connected to the benzene ring and azole ring of PATO acts as a hydrogen

Table 1 Single crystal information of PATO-N

Items	PATO-N
Chemical formula	$C_8H_6N_8O_9$
CCDC	2434866
Formula weight	358.21
Crystal size (mm^3)	0.26 × 0.23 × 0.22
Temperature (K)	150.0 (1)
Radiation	MoKα (λ = 0.71073)
Crystal system	Orthorhombic
Space group	$Pca2_1$
a (Å)	19.0525 (8)
b (Å)	4.9314 (3)
c (Å)	14.2572 (7)
α (°)	90
β (°)	90
γ (°)	90
Volume (Å^3)	1339.54 (12)
Z	4
ρ (calc.) (g cm^{-3})	1.776

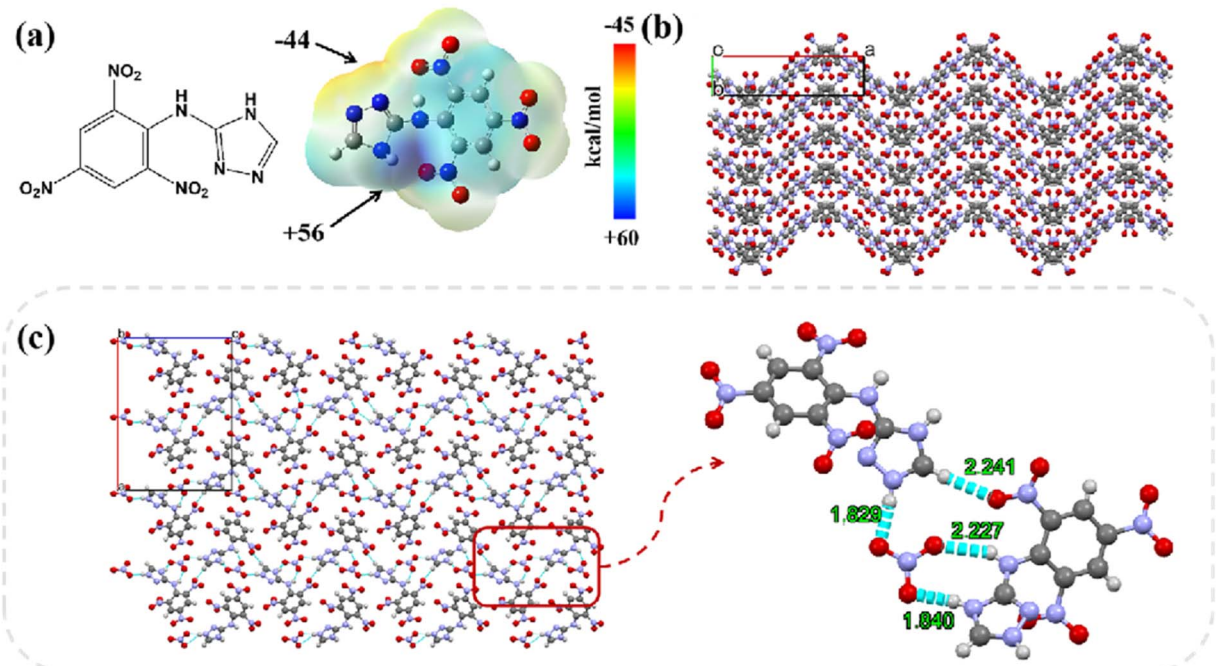

Fig. 1 (a) Molecular surface electrostatic potential of PATO, (b) *c*-axis stacking pattern of PATO-N, (c) hydrogen bond network of PATO-N.

bond donor to form a medium-strength hydrogen bond N_4–$H_4\cdots O_7$ (2.227 Å, 147.78°) with the oxygen atom on the nitrate (Table S1). This hydrogen bonding reaction is consistent with the ESP analysis results for PATO.

3.2 Hirshfeld surface analysis

Hirshfeld surface analysis[49] was employed to deconvolute the weak intermolecular interactions in the PATO-N crystal, and the results are shown in Fig. 2. The intermolecular interaction 2D fingerprint reflects the interaction between molecules in the structure and the contribution of each mode of action to the overall effect. In the PATO-N crystal system, the O–H/H–O interactions constitute the most significant intermolecular contacts, contributing 40.6% of the total Hirshfeld surface area. This indicates the importance of hydrogen bonding in maintaining the stability of the PATO-N crystal structure. The second most prominent contact is the O–O interaction, accounting for 19.2%, which mainly occurs in the light green middle region of the 2D fingerprint area. The N–O/O–N and C–O/O–C interactions are also important components, accounting for 13.8% and 13.3%, respectively.

3.3 X-ray powder

The pure PATO material and the self-assembled PATO-N material were tested using XRD. The test results are shown in Fig. 3. As can be seen, the diffraction peak of PATO is wider and the peak intensity is lower, owing to the low crystallinity; the main characteristic diffraction peaks are located at 15°, 18°, 20.3°, 23.3°, 26.2°, and 28.8°. The self-assembled PATO-N material has good crystallinity, sharp diffraction peaks, and high peak intensity. The main characteristic diffraction peaks are located at 20.6°, 22.1°, 23.3°, 26.2°, and 28.5°. The diffraction peak positions of the two materials are different, indicating that the self-assembled PATO-N material and the pure PATO material have different crystal cell structures.

3.4 Thermal stability

The thermal stability of PATO and PATO-N was further investigated through TG-DSC analysis. As shown in Fig. 4, PATO exhibits a weak endothermic peak starting at 170 °C, with a peak value of 174.6 °C, corresponding to its melting point. The

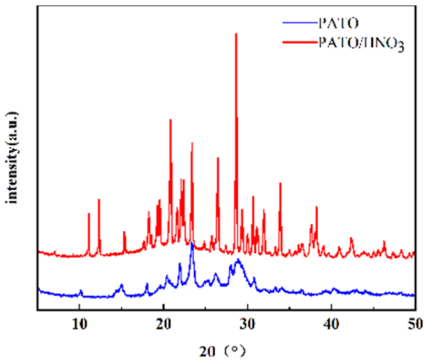

Fig. 3 X-ray diffraction patterns of PATO and PATO-N.

first strong exothermic peak appeared at 322.4 °C, reaching 327.8 °C and the second weak exothermic peak appeared at 369.8 °C, reaching 398.8 °C, which indicates that PATO was decomposed in two steps. During the decomposition step, the mass loss rate is 91.7% (Fig. S7). PATO-N began to exhibit an exothermic peak at 152.3 °C, reaching 159.3 °C, corresponding to the decomposition of nitric acid, where the mass loss rate is 13.1% (Fig. S8). An exothermic peak appeared at 266.1 °C, reaching 315.9 °C, corresponding to the decomposition of

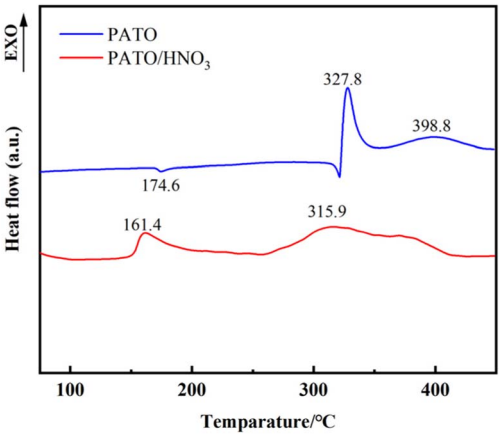

Fig. 4 DSC curves of PATO and PATO-N.

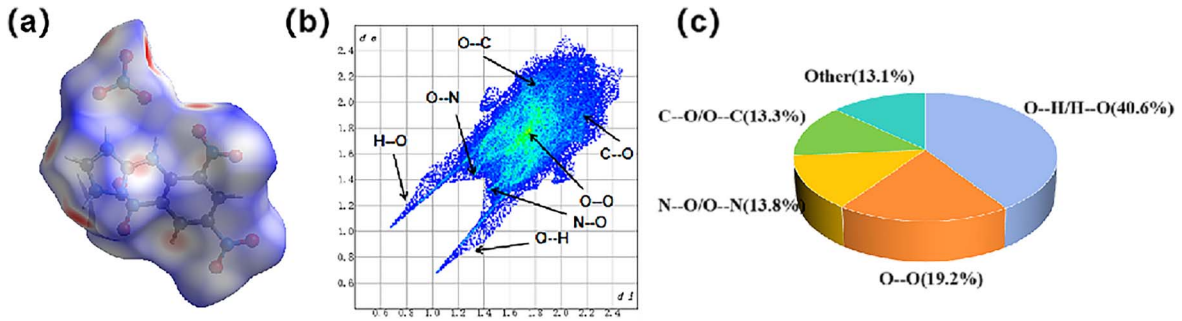

Fig. 2 (a) Hirshfeld surface of PATO-N, (b) 2D fingerprint of PATO-N, (c) individual atomic contact percentage contribution of PATO-N.

Table 2 Physiochemical properties of PATO and PATO-N

Compound	ρ (g cm^{-3})	$\Delta_f H_m$ (kJ mol^{-1})	OB (%)	D_v (km s^{-1})	P (Gpa)	IS (cm, height for 50% explosion)	T_d (°C)
PATO	1.75[a]	147.1 (ref. 48)	−67.70	7.2	20.8	137 (ref. 45)	327.8
PATO-N	1.77	76.80	−44.60	7.8	25.2	>112.2	315.9

[a] Density measured using a gas hydrometer at 295 K.

PATO-N. Compared with pure PATO, the decomposition temperature of PATO-N decreased by 11.9 °C.

3.5 Detonation performance prediction and sensitivity test

The heat of formation of energetic materials is an important parameter to evaluate the performance and stability of detonation. The enthalpy of formation of the solid state is an indispensable data to calculate the detonation velocity and pressure. However, it is often difficult to measure the energetic materials. Theoretical calculation is an important method to study the properties of energetic materials.[50]

In this paper, the enthalpy of PATO-N formation was determined through calculations in the Gaussian software. The geometric optimization of PATO-N was carried out at the B3YLP/6-311G theoretical level, and the vibration frequency calculation was carried out to obtain the zero point vibration energy. The single point energy of the molecule was calculated at the MP2/6-311++G(d,p) theoretical level. The enthalpy of formation was calculated to be +76.8 kJ mol^{-1} by the isobond reaction method after reading the thermodynamic values and electron energy, respectively. The OB of PATO and PATO-N were calculated as −67.7% and −44.6%, respectively, using the OB calculation formula, indicating that the self-assembly of the oxidizing molecular nitric acid and PATO led to improved OB. Furthermore, detonation velocity and detonation pressure were predicted with the EXPLO5 program (Table 2). According to the measured density of PATO and the enthalpy of formation provided in literature,[47] its detonation pressure and detonation velocity were calculated as 20.8 GPa and 7.2 km s^{-1}. Combined with the density and formation enthalpy of the crystal, the detonation velocity and detonation pressure of PATO-N were calculated as 7.86 km s^{-1} and 27.2 GPa. Compared with PATO, the detonation velocity and detonation pressure of PATO-N were improved. The main reason for this is the self-assembly of PATO with the oxidizing molecule nitric acid to form a supramolecular structure. The overall OB was increased by 23.1%, alleviating the limitation of energy release. The impact sensitivity (H_{50}) of PATO-N exceeds 112.2 cm, the explosive exhibits good mechanical sensitivity.

4 Conclusion

In summary, the self-assembled energetic material PATO-N, prepared through intermolecular assembly of PATO with oxidant HNO_3, crystallizes in the orthorhombic system with a $Pca2_1$ space group and exhibits a wavy molecular stacking pattern stabilized by strong hydrogen bonds, leading to enhanced structural stability. The storage temperature and humidity can significantly affect PATO-N, so it is advisable to store it sealed at room temperature. The peak temperature difference between the mixed component and the single component is 8.3 °C. According to the standards established by STANAG 4147,[51] the compatibility of PATO-N with CL-20 is considered boundary compatibility, which may be attributed to PATO-N's acidity. The thermal stability of PATO and PATO-N was investigated using TG-DSC. The decomposition temperature of PATO was 327.8 °C, while that of PATO-N was 315.9 °C, both compounds show high thermal stability. The characteristic drop height (H_{50}) for PATO-N exceeds 112.2 cm. The new energetic compound prepared possesses excellent detonation pressure and detonation velocity (P: 25.6 Gpa, D: 7.8 km s^{-1}), which is remarkably higher than those of TNT.

Author contributions

X. Zhang: conceptualization, methodology and writing original draft. Q. Zhang and Y. Zhao: writing review & editing, methodology and date analysis. G. Li and T. Jiang: methodology, XRD and DSC measurements. Z. Suo: supervision, writing review & editing. S. Sun and L. Su: conceptualization, supervision, funding acquisition, writing review & editing. All authors have read and agreed to the published version of the manuscript.

Conflicts of interest

There are no conflicts to declare.

Data availability

CCDC 2434866 contains the supplementary crystallographic data for this paper.[52]

The authors confirm that all data supporting this study are available within the article and its SI. Supplementary information is available. See DOI: https://doi.org/10.1039/d5ra05291b.

Acknowledgements

This work was supported by the PhD Project of Southwest University of Science and Technology (No. 22zx7134).

Notes and references

1 Z. Y. Yi, Y. F. Jiang, W. G. Qu, H. X. Gao and F. Q. Zhao, *Chin. J. Explos. Propellants*, 2025, **48**, 64.

2 N. V. Muravyev, D. R. Wozniak and D. G. Piercey, *J. Mater. Chem. A*, 2022, **10**, 11054.
3 X. Y. Miao, X. B. Yang, Y. C. Li and S. P. Pang, *Phys. Chem. Chem. Phys.*, 2023, **25**, 18523.
4 N. V. Muravyev, L. Fershtat and Q. H. Zhang, *Chem. Eng. J.*, 2024, **486**, 1385.
5 Y. X. Ou, *Explosives*, Beijing institute of technology press, Beijing, 2014.
6 Y. L. Zhang, Y. Liu, P. Song, H. Z. Liang, D. Yang, L. Han, H. Y. Jiang and K. Zhong, *Def. Technol.*, 2025, **48**, 238.
7 M. Lu, F. Yang and F. X. Wang, *Chin. J. Energ. Mater.*, 2025, **33**, 419.
8 M. H. Keshavarz, Y. H. Abadi, K. Esmaeilpour, S. Damiri and M. Oftadeh, *Propellants, Explos., Pyrotech.*, 2017, **42**, 1155.
9 S. P. Zhou, X. Y. Zhou and G. Tang, *J. Therm. Anal. Calorim.*, 2020, **140**, 2529.
10 P. Bhatia, P. Das and D. Kumar, *ACS Appl. Mater. Interfaces*, 2024, **16**, 64846.
11 Q. Wang and M. Lu, *New J. Chem.*, 2022, **46**, 6690.
12 D. Z. Guo, S. V. Zybin, A. P. A. Chafin and W. A. Goddard, *ACS Appl. Mater. Interfaces*, 2022, **14**, 5257.
13 L. Pei, Q. Lai, P. Yin and S. P. Pang, *Cryst. Growth Des.*, 2023, **23**, 3595.
14 Y. F. Zhou, H. X. Gao and J. M. Jeanne, *Energ. Mater. Front.*, 2020, **1**, 2.
15 Z. J. Yang, F. Y. Gong and L. Ding, *Propellants, Explos., Pyrotech.*, 2017, **42**, 809.
16 W. X. Bian, Y. N. Li, P. Peng and B. L. Wang, *J. Energ. Mater.*, 2024, DOI: **10.1080/07370652.2024.2316148**.
17 K. H. Jia, Y. C. Liu, T. Chai, Y. W. Yu, S. M. Jing, P. F. Wu, J. X. He and W. Zhang, *Propellants, Explos., Pyrotech.*, 2023, **47**, e20200279.
18 H. Kang, J. W. Kim, J. R. Lee and S. Kwon, *Combust. Flame*, 2019, **210**, 43.
19 M. N. Makhov, *Russ. J. Phys. Chem. B*, 2024, **18**, 1036.
20 B. Kramarczyk, M. Pytlik, P. Mertuszka, K. Jaszcz and T. Jarosz, *Materials*, 2022, **15**, 900.
21 B. Zhang, Y. W. Lu, Z. Li, C. Y. Li, Q. Wang, Y. J. Huang and C. P. Guo, *Propellants, Explos., Pyrotech.*, 2024, e202400146.
22 S. W. Zhang, P. C. Zhang, Z. Wang, W. L. Peng, L. H. Tan and X. G. Zhang, *Acta Armamentarii*, 2024, **45**, 147.
23 L. Zhang, C. C. Wu, Z. H. Wang, S. W. Li, S. Wang and X. Y. Guo, *Explos. Mater.*, 2022, **51**, 7.
24 J. Zhang, B. J. Tan, Q. Zhang, S. Chen, Y. X. Tang and N. Liu, *Prog. Nat. Sci.: Mater. Int.*, 2024, **34**, 1132.
25 I. Hisaki, X. Chen, K. Takahashi and T. Nakamura, *Angew. Chem., Int. Ed.*, 2019, **58**, 11160.
26 S. W. Song, Y. Wang, W. He, K. C. Wang, M. Yan, Q. L. Yan and Q. H. Zhang, *Chem. Eng. J.*, 2020, **395**, 125114.
27 X. E. Jiang, Y. Wang, W. He, K. C. Wang, M. Yan, Q. L. Yan and Q. H. Zhang, *Cryst. Growth Des.*, 2022, **23**, 333.
28 Y. Liu, Q. J. Guo, X. F. Yuan, S. B. Feng, S. F Zhu, Y. H. Chen, R. J. Gou, S. H. Zhang, Y. G. Xu and M. Lu, *J. Mol. Struct.*, 2023, **1288**, 135767.
29 Y. Li, Y. T. Cao, S. W. Song, S. T. Chen, Y. Wang, K. C. Wang and Q. H. Zhang, *Chem. Eng. J.*, 2022, **442**, 136326.
30 Y. L. Yang, Z. H. Qu, X. Y. Li, H. Y. Du, Y. F. Qin, B. Wu and K. C. Wang, *Chin. J. Explos. Propellants*, 2024, **47**, 881.
31 X. Y. Miao, X. B. Yang, Y. C. Li and S. P. Pang, *Phys. Chem. Chem. Phys.*, 2023, **25**, 18523.
32 X. B. Yang, C. H. Jia, X. Y. Miao, Y. C. Li and S. P. Pang, *RSC Adv.*, 2023, **13**, 2600.
33 A. K. Yadav, M. Jujam, V. D. Ghule and S. Dharavath, *Chem. Commun*, 2023, **59**, 4324.
34 J. X. Cai, C. P. Xie, J. Xiong, J. Y. Zhang, P. Xin and S. P. Pang, *Chem. Eng. J.*, 2022, **433**, 134480.
35 S. H. Li, S. P. Pang, X. T. Li, Y. Z. Yu and X. Q. Zhao, *Chin. Chem. Lett.*, 2007, **18**, 1176.
36 W. J. Yao, Y. B. Xue, L. Qian, H. W. Yang and G. B. Cheng, *Energ. Mater. Front.*, 2021, **2**, 131.
37 D. X. Chen, H. L. Xiong, H. W. Yang, J. Tang and G. B. Cheng, *FirePhysChem*, 2021, **1**, 71.
38 H. X. Gao and J. M. Shreeve, *Chem. Rev.*, 2011, **111**, 7377.
39 Y. Peng, Q. Yu and W. Yi, *ACS Appl. Mater. Interfaces*, 2024, **16**, 63419.
40 L. S. Gong, G. Chen, Y. Liu, T. W. Wang, J. G. Zhang, X. Y. Yi and P. He, *New J. Chem.*, 2021, **45**, 22299.
41 J. P. Agrawal and V. S. Dodke, *FirePhysChem*, 2023, **3**, 1.
42 M. D. Coburn and T. E. Jackson, *J. Heterocycl. Chem.*, 1968, **5**, 199.
43 A. O. Yigiter, M. K. Atakol, L. Aksu and O. Atakol, *J. Therm. Anal. Calorim.*, 2017, **127**, 2199.
44 L. Türker and Ç. Ç. Çelik Bayar, *Z. Anorg. Allg. Chem.*, 2012, **638**, 1316.
45 J. P. Agrawal, U. S. Prasad and R. N. Surve, *New J. Chem.*, 2000, **24**, 583.
46 P. Leonard, P. Bowden, M. Shorty and M. Schmitt, *Propellants, Explos., Pyrotech.*, 2019, **44**, 203.
47 J. P. Agrawal, *Cent. Eur. J. Energ. Mater.*, 2012, **9**, 273.
48 Z. L. Chioato, T. M. Klapötke, F. Mieskes, J. Stierstorfer and M. Weyrauther, *Eur. J. Inorg. Chem.*, 2016, **7**, 956.
49 P. R. Spackman, M. J. Turner, J. J. McKinnon, S. K. Wolff, D. J. Grimwood, D. Jayatilaka and M. A. Spackman, *Appl. Crystallogr.*, 2021, **54**, 1006.
50 Z. X. Zhang, L. Y. Wen, T. Yu, C. Chen, S. V. Bondarchuk and Y. Z. Liu, *Fule*, 2026, **404**, 136307.
51 J. S. Li, J. J. Chen, C. C. Hwang, K. T. Lu and T. F. Yeh, *Propellants, Explos., Pyrotech.*, 2019, **44**, 1270.
52 X. Zhang, Q. Zhang, Y. Zhao, G. Li, T. Jiang, Z. Suo, S. Sun and L. Su, CCDC 2434866: Experimental Crystal Structure Determination, 2025, DOI: **10.5517/ccdc.csd.cc2mqp24**.